J Mater Sci: Mater Electron (2010) 21:1229–1234
DOI 10.1007/s10854-009-0051-9

Structural, optical, electrical and morphological properties of ZnTe films deposited by electron beam evaporation

M. G. Syed Basheer Ahamed · V. S. Nagarethinam · A. Thayumanavan · K. R. Murali · C. Sanjeeviraja · M. Jayachandran

Received: 5 October 2009 / Accepted: 28 December 2009 / Published online: 7 January 2010

Abstract ZnTe films were deposited on glass substrates at different substrate temperatures in the range 30–300 °C. The thickness of the films was about 200 nm. The films exhibited cubic structure with preferential orientation in the (111) direction. Band gap values in the range 2.34–2.26 eV are observed with increase of the substrate temperature. The refractive index values are in the range of 2.55–2.92 for the films deposited at different substrate temperatures. It is observed that the conductivity increases continuously with temperature. Laser Raman studies indicated the presence of peaks at 206.9 and 412.2 cm^{-1}corresponding to the first order and second order LO phonon.

1 Introduction:

The II–VI compound semiconductors have attracted many researchers, over the years, because of their possible applications in the fabrication of solar cells, light emitting diodes (LEDs), photo diodes, photo detectors and many other opto-electronic devices. Zinc Telluride (ZnTe) is one of the important members of the II–VI group, having electrical and optical properties suitable for the fabrication of various opto-electronic devices. It has a wide and direct bandgap of 2.26 eV (at room temperature) [1, 2] which is in the pure green region of the electromagnetic spectra. This direct bandgap of 2.26 eV makes it a potential candidate for the fabrication of pure green LEDs [3–6]. Because of its high electro-optic coefficient, ZnTe also promises to be useful in the production and detection of terahertz (THz) radiation [3, 7]. Since there is only a small valence band offset of 0.1 eV between ZnTe and CdTe, ZnTe can be used as a back contact material to obtain higher efficiency in CdTe based solar cells [8]. Though some research groups have reported the fabrication of ZnTe based devices like LEDs and THz detectors, most of them have preferred higher-end methods like molecular beam epitaxy (MBE), metal organic chemical vapor deposition (MOCVD), etc. to obtain ZnTe films [3–8], or electrodeposition from aqueous solutions [9, 10]. ZnTe is a very attractive host for optoelectronic device realizations because of its direct bandgap in the green spectral range (2.26 eV). Specifically, for bright LEDs, ZnTe is an interesting candidate since the emission wavelength corresponds to the maximum sensitivity of the human eye. Employment of ZnTe were reported by the realization of LED prototypes [11, 12], high-efficiency multi-junction solar cells [13], and THz devices [14]. In some former studies the concept of laser crossing and all-optical laser transmission digitizing with GaAs [15, 16], CdS [17] and InP has been demonstrated [18]. In an earlier report on electron beam evaporated ZnTe films, the optical and dielectric properties were discussed [19]. The exploration of novel solutions, materials and simple technologies for future light-based communication systems, such as all-optical switches and hybrid device structures [20], have

M. G. Syed Basheer Ahamed
MIET Arts and Science College, Trichy 620007, India

V. S. Nagarethinam · A. Thayumanavan
Department of Physics, A.V.V.M Sri Pushpam College, Poondi, India

K. R. Murali · M. Jayachandran (✉)
Electrochemical Materials Science Division, Central Electrochemical Research Institute, Karaikudi 630006, India
e-mail: mjayam54@yahoo.com

C. Sanjeeviraja
Department of Physics, Alagappa University, Karaikudi 630003, India

been the driving motivation for the current work. In this study, structural, optical, morphological and electrical properties of ZnTe films deposited by the electron beam (EB) evaporation are presented and discussed.

2 Experimental

Thin ZnTe films were deposited using Hind Hivac electron beam evaporation unit on glass substrates at different temperatures in the range 30–300 °C. Commercial ZnTe powder (99.99% purity) was used as the source. Deposition rate was fixed as 40 nm/min. The evaporation conditions were: (1) a vacuum of 10^{-6} Torr; (2) an accelerating voltage of 5 kV; and (3) electron beam current 10 mA. The substrate temperature was fixed based on the DTA results which indicated an exothermic peak at 437 °C due to the partial evaporation of ZnTe. The films were characterized by x-ray diffraction (XRD) studies using CuKα radiation from an Xpert PANanalytical XRD unit. Optical studies were made at room temperature using a UV–Vis-NIR spectrophotometer. Surface morphology of the films was studied by Molecular Imaging system atomic force microscope. Raman studies were made using Renishaw Invia Laser Raman microscope using a 18 mW 633 nm He–Ne laser. Electrical resistvity was evaluated by providing Al contact.

3 Results and discussion:

The x-ray diffraction pattern (Fig. 1) shows that the ZnTe films deposited at various substrate temperatures posses cubic structure with an average lattice contant 'a' = 6.093 Å. The different peaks were indexed and the corresponding interplanar spacing 'd' were calculated and compared with the standard ASTM values given in ASTM card No 15-746. Preferential orientation in the (111) direction is also observed. The films deposited at room temperature indicate amorphous structure. As the deposition temperature increased, the peaks became sharper suggesting improved crystallinity. The thickness of the films estimated from Mitrutoyo surface profilometer was about 200 nm. The microstructural parameters like grain size, strain, dislocation density and number of crystallites have been calculated and are indicated in Table 1. From the table, it is observed that grain size increases with substrate temperature. The dislocation density decreases with increase of substrate temperature. The substrate temperature plays a vital role in deciding the microstructural parameters of ZnTe films. First, due to the increase in crystallite grain size with substrate temperature, the defects in the crystalline lattice is greatly reduced which subsequently reduces the strain. Further, as the substrate

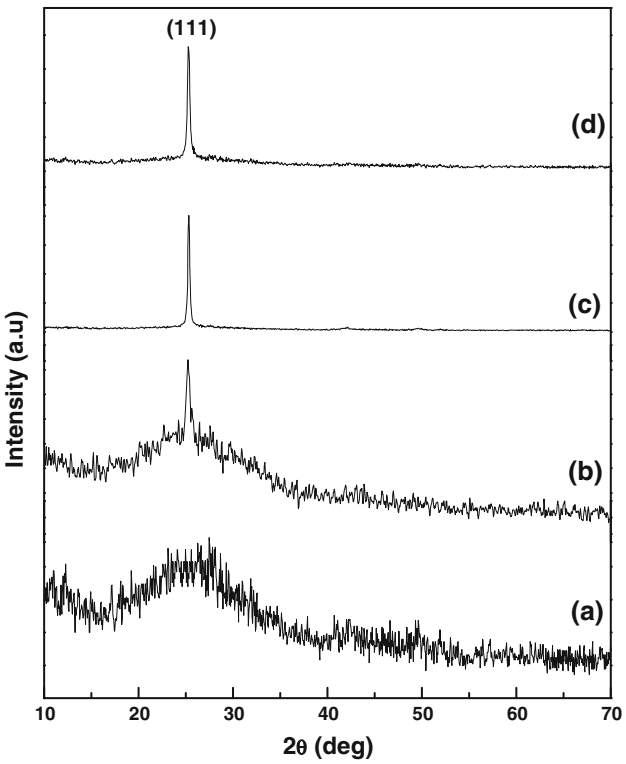

Fig. 1 XRD patterns for the ZnTe films deposited at different substrate temperatures **a** RT, **b** 100 °C, **c** 200 °C and **d** 300 °C

temperature increases, stress developed is reduced within the film and also the dislocation density decreases. Owing to the release of stress in the films, the variation of interplanar spacing leads to a decrease in the defects and the related microstrain. Also the peak width(FWHM) decreased with increasing temperature. The increase in peak intensity and decrease of FWHM is due to the improvement in the crystallinity and a reduction in the microstrain [21]. It is observed that the particle size increases with increased deposition temperature and reached a maximum value of 43.2 nm at a temperature of 300 °C. Due to the increase of particle size with deposition temperature, the defects in the lattice is decreased, which in turn reduces the stress, internal microstrain and dislocation devsity [21, 22]. Similar structural dependence of the microstructural parameters on the deposition of other materials have been reported [22, 23].

The variation of absorbance with wavelength was studied for the ZnTe films deposited at different substrate temperatures. All the films exhibit a similar behaviour in the wavelength range of 1000–2500 nm. The onset of absorption is observed in the range 650–550 nm depending upon the substrate temperature. A very high value of absorption co-efficient (10^4 cm^{-1}) is observed for all the films. Plots of $(\alpha h\nu)^2$ versus $h\nu$ (Fig. 2) yielded band gap values in the range 2.34–2.26 eV as the substrate

Table 1 Lattice parameter, grain size, strain, stress and dislocation density of ZnTe films deposited at different substrate temperatures

Substrate temperature (°C)	Lattice parameter "a" (Å)		Grain size (nm)	Stress ($\times 10^{10}$) dyne cm^{-2}	Strain ($\times 10^{-4}$)	Dislocation density ($\times 10^{16}$ cm^{-3})
	Standard	Calculated				
30	6.1037	6.084	18.6	4.37	11.2	0.447
100		6.092	28.7	−1.78	7.2	0.058
200		6.094	34.6	−0.91	6.1	0.043
300		6.102	43.2	−0.89	4.8	0.027

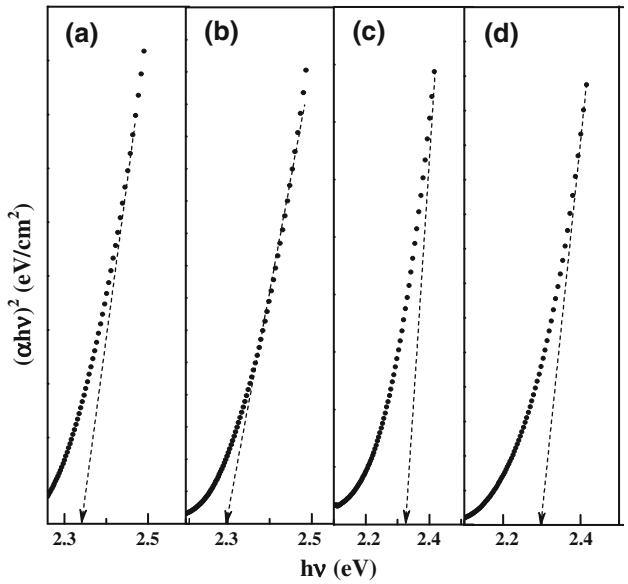

Fig. 2 $(\alpha h\nu)^2$ versus $h\nu$ plot for the ZnTe films deposited at different substrate temperature **a** RT, **b** 100 °C, **c** 200 °C and **d** 300 °C

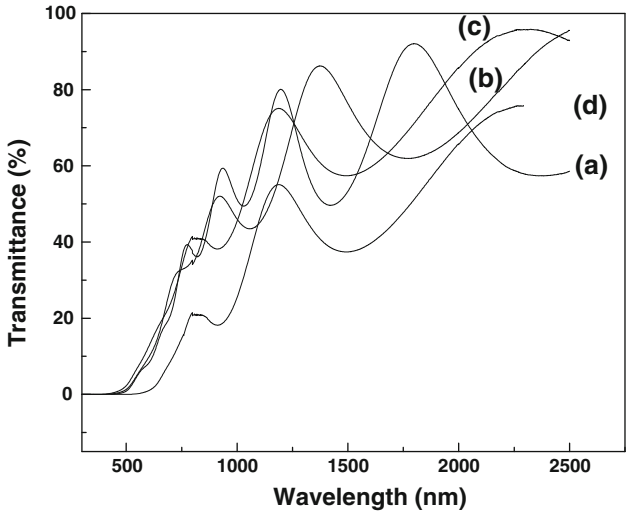

Fig. 3 Optical transmittance spectra of ZnTe films deposited with different substrate temperatures **a** RT **b** 100 °C **c** 200 °C and **d** 300 °C

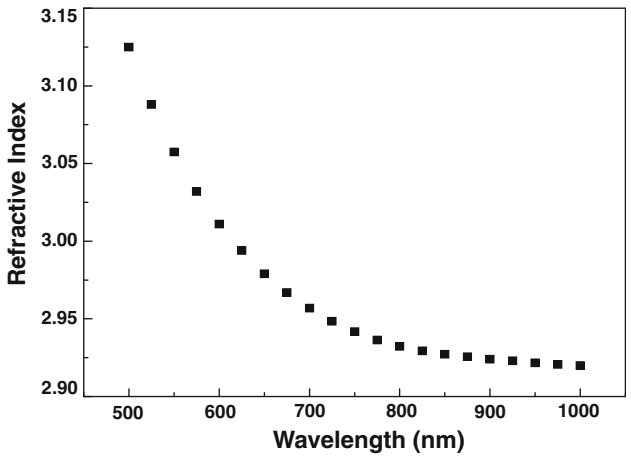

Fig. 4 Refractive index graph for the ZnTe films deposited at 300 °C

temperature increased. The lower value of the band gap at higher substrate temperatures is due to the large grain size developed at higher temperature. Figure 3 presents the optical transmittance spectra of the ZnTe films deposited at different temperatures. Interference fringes are observed in these films which confirms the formation of smooth and uniform films. The refractive index was calculated using the interference maxima and minima observed at a wavelength from the transmission spectra by the envelope method [22] employing the following equations:

$$n = [N + (N^2 - n_s^2)]^2 \quad (1)$$

$$N = (n_s^2 + 1)/2 + 2n_s(T_{max} - T_{min})/T_{max}T_{min} \quad (2)$$

where n_s is the refractive index of the substrate, T_{max} and T_{min} are the maximum and minimum transmittances at the same wavelength in the fitted envelope curve on a transmittance spectrum.

The variation of refractive index with wavelength is shown in Fig. 4. The refractive index decreases with increasing wavelength. The values of refractive index are constant in the near infrared region. The refractive index values are in the range of 2.55–2.92 for the films deposited at different substrate temperatures. These values are comparable to earlier reports [23].

Surface morphology of the films deposited at different substrate temperatures was studied by Atomic force

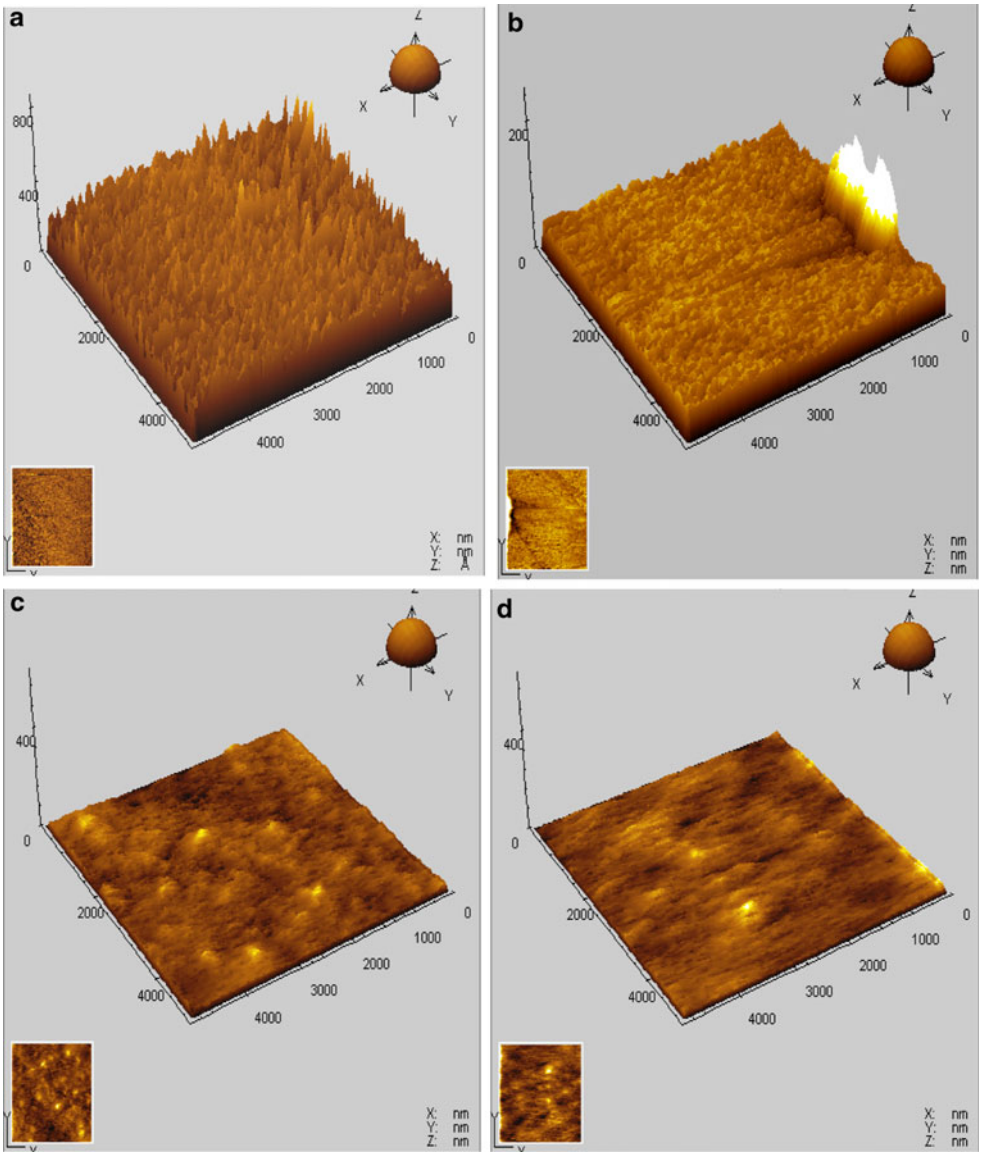

Fig. 5 Three dimensional (3D) topographic AFM images of ZnSe fims deposited at different substrate temperature **a** RT, **b** 100 °C, **c** 200 °C and **d** 300 °C

microscope (AFM). Figure 5 shows the AFM micrographs. The presence of nanocrystallites is evident from the figure. The grain size and the root mean square (RMS) value of the roughness varies from 60 to 120 nm and from 2.1 to 0.9 nm respectively with increase of substrate temperature.

Composition of the films was estimated from Energy dispersive analysis of x-rays (EDAX). The ratio of Zn:Te are 48.8:51.2, 49.5:50.5, 49.1:50.9 and 49.3:50.7 for the films deposited at different substrate temperatures (Fig. 6).

Variation of resistivity with temperature was measured as a function of temperature in the range of 27–150 °C (Fig. 7) for the films of deposited at different temperatures 30,100, 200 and 300 °C. It is observed that the conductivity changes continuously with temperature. A thermally activated conduction mechanism is observed. The conductivity can be represented by

$$\sigma = \sigma_0 \exp(-\Delta E_\sigma / K_B T)$$

where ΔE_σ is the activation energy, T is the temperature, K is the Boltzmann constant. The plot exhibits two slopes. The low activation energies are due to the high resistance of the samples. When the temperature increases, the activation energy also increases.

The room temperature Raman spectra of ZnTe films are shown in Fig. 8 for the films of different thicknesses and deposited at a substrate temperature of 200 °C. The first order Raman scattering of a crystalline material with cubic structure usually shows two peaks corresponding to the Transverse optic (TO) and longitudinal optic (LO) zone-centre phonon modes [24]. The presence of peaks at 206.9 and 411.9 cm^{-1} is assigned to the first order and second order ZnTe LO phonon scattering. The peak at 233.7 eV could not be associated either with ZnTe or Te precipitates.

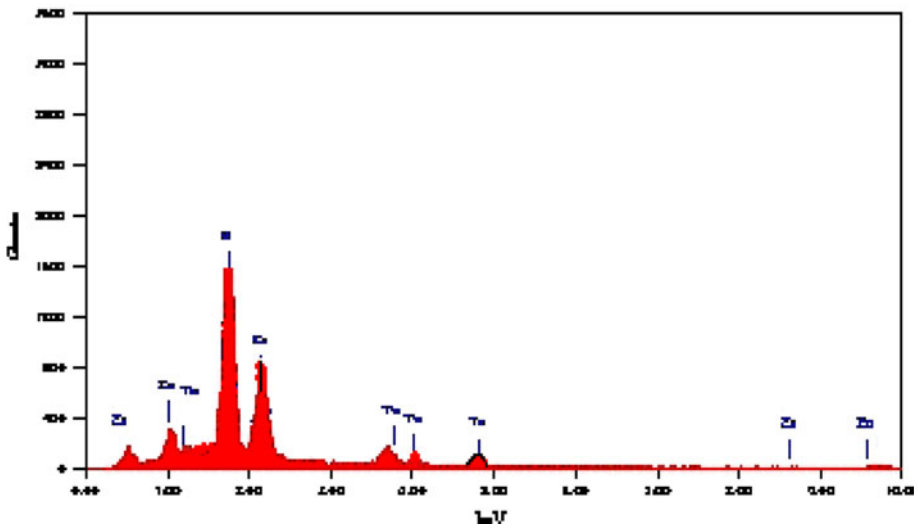

Fig. 6 EDAX spectra for the ZnTe films deposited at 300 °C

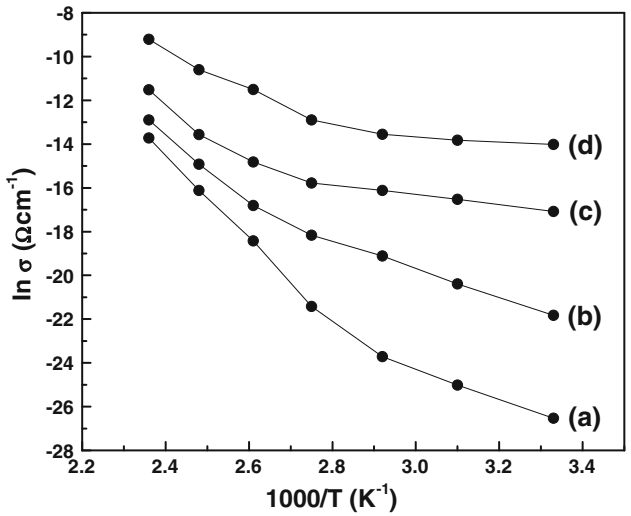

Fig. 7 ln σ versus 1/T curves for ZnTe films deposited at different substrate temperatures **a** RT **b** 100 °C **c** 200 °C and **d** 300 °C

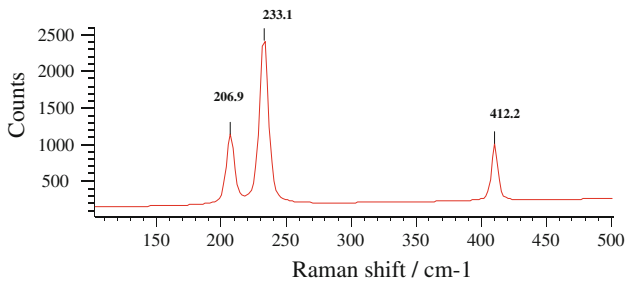

Fig. 8 Raman spectra for the ZnTe films deposited at 300 °C

4 Conclusion:

The results of this study indicate that uniform and device quality ZnTe films with cubic structure can easily be deposited by the EB evaporation technique. Films with direct band gap in the range of 2.26–2.34 eV can be deposited. Films with grain size in the range 60–120 nm can be obtained.

References

1. K.P. Acharya, A. Erlacher, B. Ullrich, Thin Solid Films **515**, 4066 (2007)
2. A.A. Ibrahim, N.Z. El-Sayed, M.A. Kaid, A. Ashour, Vacuum **75**, 189 (2004)
3. C.X. Shan, X.W. Fan, J.Y. Zhang, Z.Z. Zhang, X.H. Wang, J.G. Ma, J. Vac. Sci. Technol. **20**, 1886 (2002)
4. A. Ueta, D. Hommel, Phys. Stat. Sol. **A192**, 177 (2002)
5. K. Yoshino, A. Memon, M. Yoneta, K. Ohmori, H. Sato, M. Ohishi, Phys. Stat. Sol. (B) **229**, 977 (2002)
6. J.H. Chang, T. Takai, K. Godo, J.S. Song, B.H. Koo, T. Hanada, Phys. Stat. Sol. (B) **229**, 995 (2002)
7. Q. Guo, Y. Kume, Y. Fukuhara, T. Tanaka, M. Nishio, H. Ogawa, Solid State Commun. **141**, 188 (2007)
8. B. Spath, J. Fritsche, F. Sauberlich, A. Klein, W. Jaegermann, Thin Solid Films **480**, 204 (2005)
9. T. Ishizaki, T. Ohtomo, A. Fuwa, J. Electrochem. Soc. **151**, C161 (2004)
10. T. Ishizaki, N. Saito, O. Takai, S. Asakura, K. Goto, A. Fuwa, Electrochim. Acta **50**, 3509 (2005)
11. K. Yoshino, A. Memon, M. Yoneta, K. Ohmori, H. Saito, M. Ohishi, Phys. Status Solidi. (B) **229**, 977 (2002)
12. K. Sato, M. Hanafusa, A. Noda, A. Arakawa, M. Uchida, T. Asahi, O. Oda, J. Cryst. Growth **214/215**, 1080 (2000)
13. D. Rioux, D.W. Niles, H. Hochst, J. Appl. Phys. **73**(12), 8381 (1993)
14. K. Liu, H. Kang, T. Kim, X.-C. Zhang, Appl. Phys. Lett **81**, 4115 (2002)
15. A. Erlacher, B. Ullrich, Semicond. Sci. Technol. **19**, L9 (2004)
16. B. Ullrich, A. Erlacher, E.O. Danilov, Semicond. Sci. Technol. **19**, L111 (2004)
17. A. Erlacher, H. Miller, B. Ullrich, J. Appl. Phys **95**, 2927 (2004)
18. A. Erlacher, B. Ullrich, R.J. Konopinski, H.J. Haugan, Proc. SPIE **5723**, 179 (2005)
19. A.M. Salem, T.M. Dahy, Y.A. El-Gendy, Phys. B **403**, 3027 (2008)

20. C.X. Shan, X.W. Fan, J.Y. Zhang et al., J. Vac. Sci. Technol. A-Vac. Surf. Films **20**, 1886 (2002)
21. N. El-Kadry, A. Aahour, S.A. Mohamoud, Thin Solid Films **269**, 112 (1995)
22. H.Y. Joo, H.J. Kim, J. Vac. Sci. Technol. **A 17**, 862 (1999)
23. A.E. Merad, M.B. Kanoun, G. Merad, J. Cilat, H. Aourag, Mater. Chem. Phys **92**, 333 (2005)
24. E. Rudiger, J. Alvareg Garcia, I. Luck, J. Klaer, R. Scheer, J. Phys. Chem. Solids **64**, 1977 (2003)